Supporting Information

Electronic metal-support interaction boosts electrochemiluminescence by improving the catalytic activity of palladium

Mingtong Cai, Jiaqi Gao, Jian-Bin Pan, Li-Qing Zheng, and Jing-Juan Xu**

State Key Laboratory of Analytical Chemistry for Life Science, School of Chemistry, Nanjing University, Nanjing 210023, People's Republic of China.

*Corresponding author: Li-Qing Zheng lzheng@nju.edu.cn; Jing-Juan Xu xujj@nju.edu.cn

Contents

1. Chemicals and reagents

Palladium(II) chloride ($PdCl_2$), potassium chloride (KCl), sodium chloride (NaCl), hydrochloric acid (HCl), hydrogen peroxide (H_2O_2), lactic acid, and sucrose were acquired from Sinopharm Chemical Reagent Co., Ltd. (Shanghai, China). L-Ascorbic acid (AA), hexadecyltrimethylammonium bromide (CTAB), 5,5-dimethyl-1-pyrroline-N-oxide (DMPO) 3,3',5,5'-tetramethylbenzidine (TMB), 3,4-Dihydroxyphenethylamine (Dopamine), and fructopyranose were purchased from Aladdin Industrial Corporation (Shanghai, China). Sodium iodide (NaI) was purchased from Shanghai Bide Pharmaceutical (Shanghai, China). Glucose, uric acid, and thiourea were sourced from Macklin Biochemical Co., Ltd. (Shanghai, China). Luminol was provided by Ciens Co., Ltd. (Shanghai, China). Britton-Robinson (BR) buffer (pH 10.0), and sodium acetate buffer (pH 4.0) were supplied by Yeasen Biotechnology Co., Ltd. (Shanghai, China). Phosphate buffered saline (PBS) buffer (pH 7.5) was purchased from Solarbio Science and Technology Co.,Ltd. (Beijing, China). Graphene nanosheets, glucose oxidase (GOx), and p-Benzoquinone (p-BQ) were obtained from Meryer Biochemical Technology Co., Ltd. (Shanghai, China). All these aqueous solutions were prepared using ultrapure deionized water (18.2 MΩ·cm). All reagents are used without further purification.

2. Measurements and calculation details

The morphology of the synthesized nanoparticles was characterized by scanning electron microscope (SEM) (Hitachi S-4800, Japan). The X-ray photoelectron spectrometer (XPS) spectra were obtained by a K-Alpha X-ray photoelectron spectrometer (Thermo Fisher Scientific, USA). The position of the center of the valence band is given by the following formula

$$\varepsilon_d = \int N(\varepsilon)\varepsilon \, d\varepsilon \, / \int N(\varepsilon) \, d\varepsilon \quad \text{(S1)}$$

where $N(\varepsilon)$ is the density of states, here it refers to the XPS intensity after background subtraction, and ε is the energy of states.[1] Ultraviolet photoelectron spectroscopy (UPS) measurements was implemented using an ESCALAB Xi UV spectrometer (Thermo Fisher Scientific, USA) and the sample was biased by -5 V. The work function (φ) values were calculated based on the following equation:

$$\varphi = h\nu - (E_{cutoff} - E_{Fermi}) \quad \text{(S2)}$$

where $h\nu$ is the energy of the UV photon (He I, 21.2 eV), and E_{cutoff} is the energy of the secondary-electron cutoff.[2] Electron paramagnetic resonance (EPR) spectra were obtained by a Magnettech 5000 spectrometer (Bruker, Germany). UV absorption was measured by a Varioskan Flash (Thermo Fisher, USA).

3. Synthesis of PdNPs and Pd-GR composite

Palladium nanoparticles (PdNPs) were synthesized following a reported procedure using a seed-mediated growth in an aqueous Pd precursor suspension.[3] To prepare 11 nm-size Pd cube-shaped seeds, 45.6 mg of CTAB was dissolved in 10 mL of ultrapure water in a

20 mL glass vial equipped with a stirring bar. The solution was heated to 95 °C under stirring, followed by the addition of 0.25 mL of 20 mM H_2PdCl_4 solution. After 5 min of stirring, 0.2 mL of 0.1 M ascorbic acid solution was quickly added. The reaction mixture was stirred for 10 min at 95 °C, then cooled down to 30 °C, and allowed to age for 1 h. Separately, a solution containing 1 g of CTAB in 6.8 mL of ultrapure water was mixed with 0.25 mL of 10 mM NaI solution. Next, 3.2 mL of 100 mM H_2PdCl_4 was added. H_2PdCl_4 solution was prepared by dissolving 57.5 mg of $PdCl_2$ in 3.25 mL of 0.2 M HCl under stirring for 3 hours until a clear orange-brown solution formed. The addition of H_2PdCl_4 resulted in a turbid orange suspension, which was stirred in a water bath at 30 °C. Finally, 10 mL of the aged Pd cube-shaped seeds was added to the growth solution under vigorous stirring, followed by the addition of 5 mL of 1 M ascorbic acid. The resulting mixture was vigorously stirred at 30 °C for 6 h. The resulting PdNPs solution was centrifuged at 5000*g* for 10 min at 27 °C to remove excess CTAB and was subsequently redispersed in ultrapure water.

Graphene nanosheets were commercially available. The Pd-GR composite was prepared by mixing a dispersion of palladium nanoparticles (1.4 mg/mL) with a graphene dispersion (0.5 mg/mL) at a volume ratio of 1:3, followed by sonication for 10 minutes.

4. Preparation of the modified electrode

First, glassy carbon electrodes (GCE) were sequentially polished with 0.3 and 0.05 μm alumina powder, followed by sonication in ethanol and water for 2 minutes each. Next, 10 μL of the material dispersion was drop-casted onto the pre-treated electrode and dried at room temperature before use.

5. ECL and electrochemical measurements

ECL measurements were performed using a CHI-660E potentiostat (Chenhua Instruments, Shanghai, China) and a MPI-E multifunctional electrochemical and chemiluminescent analytical system (Xi'an Remex Electronic Science &Technology Co. Ltd., Xi'an, China). Cyclic voltammetry (CV) measurement was applied with a potential range from 0 V to +0.6 V at a scan rate of 0.1 V/s, with a three-electrode system consisting of a Ag/AgCl (saturated KCl) reference electrode, a Pt wire (0.5 mm diameter) counter electrode, and a GCE working electrode. The photomultiplier tube (PMT) was biased at -300 V. Electron paramagnetic resonance (EPR) spectroscopy was performed in methanol or H_2O containing 250 μL of Pd-GR composite, 50 μL of 100 mM H_2O_2, and 5 μL of pure 5,5-dimethyl-1-pyrroline N-oxide (DMPO), after applying a CV scan from 0 V to +0.6 V at a scan rate of 0.1 V/s. To analyze the ECL mechanism, radical scavengers were added to the electrolyte consisting of luminol and H_2O_2. 1 mM thiourea and p-benzoquinone were used to capture ·OH and $O_2^{\bullet-}$, respectively. CV curves were recorded in BR buffer solution (pH 10.0) containing 0.2 mM luminol, with a potential range from 0 V to +0.6 V at a scan rate of 0.1 V/s. Electrochemical impedance spectroscopy (EIS) measurements were carried out from 0.1Hz to 100 kHz in 5.0 mM $K_3[Fe(CN)_6]/K_4[Fe(CN)_6]$ solution containing 0.1 M KCl. The electrochemical active surface area (ECSA) was measured by CV scan in 5.0 mM $K_3[Fe(CN)_6]/K_4[Fe(CN)_6]$ (0.1 M KCl) with a potential range from -0.2 V to 0.6 V and scanning rate from 0.025 V/s to 0.25 V/s.

6. Analysis of POD-like activity

POD-like activities were measured using TMB colorimetric assays. For this measurement, 10 μL of the material dispersion was added to a mixed solution containing 50 μL of 10 mM H_2O_2, 50 μL of 10 mM TMB, and 100 μL of sodium acetate buffer (pH 4.0). After being incubated at 37 °C for 15 min, the resulting mixture was used for UV-Vis absorption measurements.

7. Density functional theory (DFT) calculations

All calculations were performed using the Vienna Ab initio Simulation Package (VASP) based on density functional theory (DFT).[4] The system consists of a graphene-supported three-layer Pd (111) slab model, with a 15 Å vacuum layer introduced to eliminate interactions between periodic layers. Electron-ion interactions were described by the projector augmented wave (PAW) pseudopotentials, and the exchange-correlation functional was treated with the Perdew-Burke-Ernzerhof (PBE) formulation within the generalized gradient approximation (GGA).[5] The plane-wave cutoff energy was set to 500 eV to ensure computational accuracy. The first Brillouin zone was sampled using a Gamma-centered Monkhorst-Pack k-point mesh, with the mesh density determined according to the system size to guarantee energy convergence. The convergence criterion for the electronic self-consistent loop was set to 10^{-8} eV in energy change, while that for ionic relaxation was set to 0.03 eV/Å in atomic forces. Considering the strong correlation effects of d electrons in Pd atoms, the DFT+U method was applied with an effective U value of 2.0 eV for the Pd d orbitals. Data preprocessing and result extraction were carried out using the VASPKIT tool. All crystal structures and electron density distributions were visualized with VESTA software. The isosurface value for the charge density difference was set to 0.005 e/Å³.

8. Detection of glucose

Aliquots of 100 μL of glucose solutions at various concentrations were added to a mixture containing 50 μL of GOx (5 U/ml) and 850 μL of PBS (pH 7.5). After thorough mixing, the reaction was allowed to proceed at 37 °C for 10 min. The resulting mixture was then used for ECL tests in a BR buffer solution (pH 10.0) containing 0.2 mM luminol, with the photomultiplier tube voltage set at -600 V. The anti-interference studies include the following substances: 1 mM KCl, 1 mM NaCl, 50 μM lactic acid, 5 μM uric acid, 5 μM dopamine, 1 mM fructose, and 1 mM sucrose. Urine samples were collected from healthy adult volunteers. The samples were stored at -20 °C without any pretreatment. Prior to analysis, the urine samples were diluted tenfold, and subsequent testing was performed following the same procedure as described above, except that the glucose solution was replaced by urine diluted tenfold.

9. Collection and preservation of urine samples

All urine samples were collected from healthy adult volunteers. Urine collection and all relevant studies were approved by the ethics committee of Nanjing University (IRB20260206012). All collected urine samples were divided into aliquots and stored at -

20 ℃ before future measurement.

10. Characterization of PdNPs

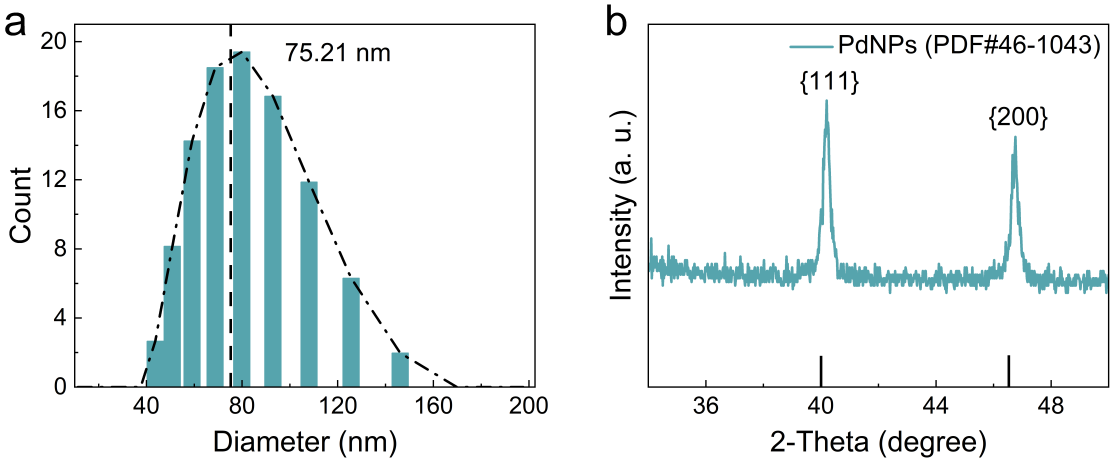

Figure S1. (a) Hydrodynamic particle size distribution of PdNPs measured by dynamic light scattering, showing the average size. (b) X-ray diffraction (XRD) spectra of PdNPs. The lower panel shows the standard XRD data (PDF#46-1043).

11. Optimization of ECL experimental conditions

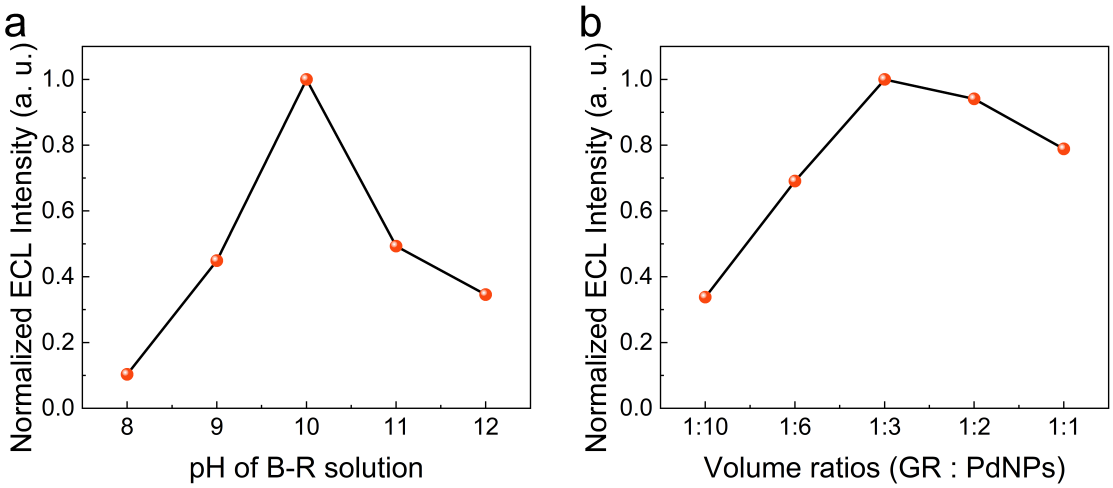

Figure S2. (a) Effect of the solution pH of BR buffer on ECL intensity obtained from the Pd-GR sample. (b) Effect of mixing volume ratios of GR and PdNPs dispersion on ECL intensity in BR buffer (pH 10.0). The ECL measurements were performed in electrolyte containing 0.2 mM luminol and 10 mM H_2O_2. PMT was biased at -300 V.

To evaluate the ECL performance of GR, PdNPs, and Pd-GR, the materials were deposited onto glassy carbon electrodes (GCE) for subsequent experiments. One of the key reactions in the luminol-H_2O_2 ECL system is the oxidation of luminol, which can be accelerated by alkaline conditions through the formation of luminol anions. Therefore, we first

optimized the pH of the electrolyte for the ECL system. The ECL intensity of luminol increases with the increase of solution pH and reaches the maximum at pH = 10.0, whereas ECL signal decreases when solution pH is above 10.0 (Figure S2a). This is likely related to the pH-dependent behavior of luminol during electrochemical oxidation.[6,7] Additionally, the volume ratio of GR and PdNPs dispersion in preparing Pd-GR composite is a critical factor in determining the interfacial structure of the obtained materials. The maximum ECL intensity was achieved at a GR : PdNPs volume ratio of 1:3 (Figure S2b) in the BR buffer solution (pH 10.0) containing 0.2 mM luminol and 10 mM H_2O_2. When the GR concentration is too high, the relatively fewer active sites of PdNPs may be covered by GR, thereby affecting the catalytic performance. On the other hand, when the concentration of PdNPs is too high, PdNPs may aggregate on the GR surface without achieving efficient contact with the GR, which significantly reduces the catalytic activity of the Pd-GR composites. Unless otherwise specified, subsequent experiments were conducted at a GR : PdNPs volume ratio of 1:3.

12. EPR spectra of $O_2^{\cdot-}$ and ·OH

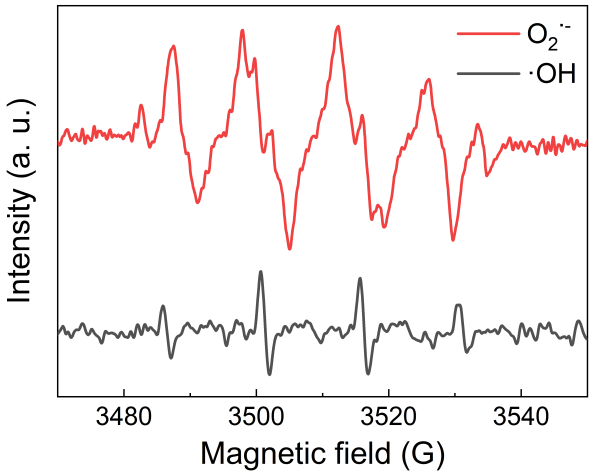

Figure S3. EPR spectra obtained from the Pd-GR sample in the BR buffer solution containing 10 mM H_2O_2, and DMPO dissolved in methanol (red line) and in H_2O (black line) as the trapping agent.

13. Radical quenching experiment on ECL intensity

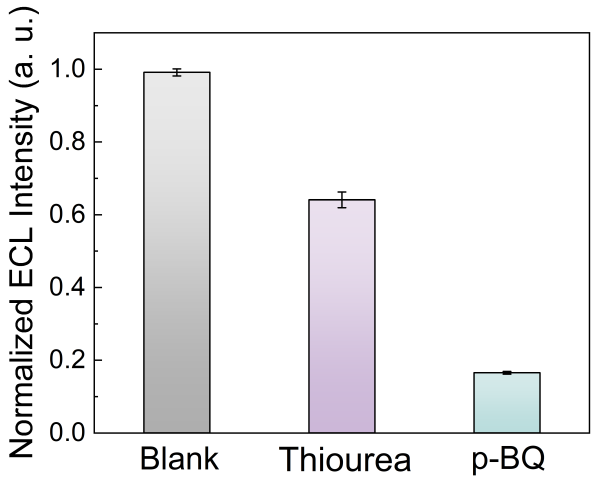

Figure S4. Effect of different radical scavengers on ECL intensity in BR buffer (pH 10.0) containing 0.2 mM luminol, 10 mM H_2O_2, and 0.1 mM radical scavengers. PMT was biased at -300 V.

14. Electrochemical activity analysis of GR, PdNPs, and Pd-GR

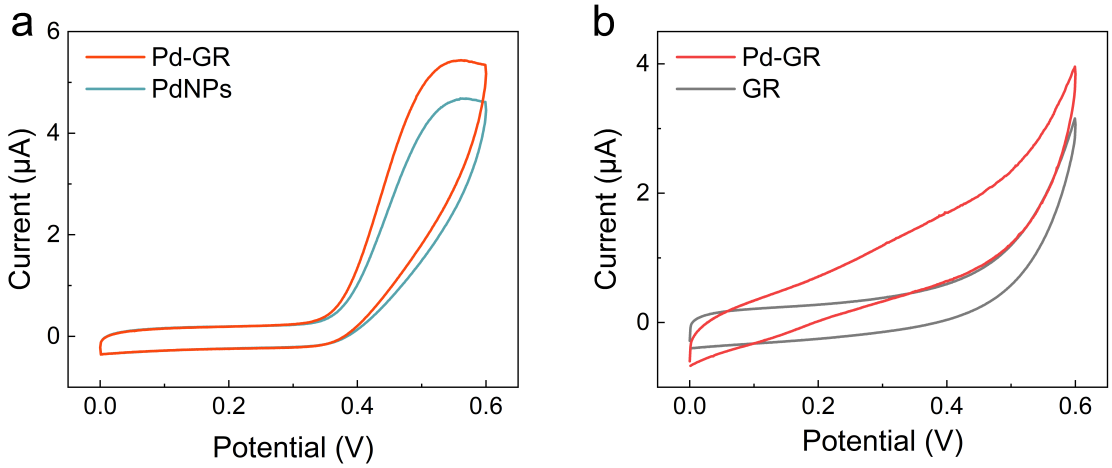

Figure S5. (a) CV curves obtained at GR-, PdNPs-, and Pd-GR-modified GCE in BR buffer (pH 10.0) containing 0.2 mM luminol. (b) CV curves obtained at GR- and Pd-GR-modified GCE in BR buffer (pH 10.0) containing 10 mM H_2O_2.

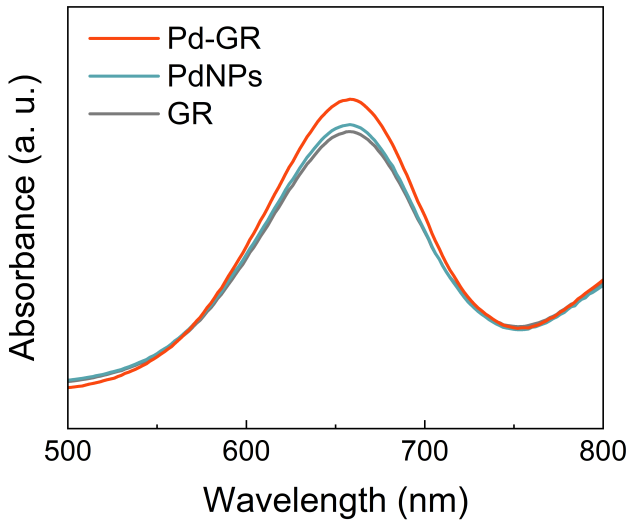

Figure S6. POD-like catalytic activity characterization by UV-vis spectrometry in sodium acetate buffer solution (pH 4.0) containing 2.4 mM TMB and 2.4 mM H_2O_2.

The peroxidase-like activities of GR, PdNPs, and Pd-GR composite were evaluated by the 3,3',5,5'-tetramethylbenzidine (TMB) chromogenic reaction assay using UV-vis absorption spectroscopy. Figure S6 shows that prominent UV-visible absorption peaks at 652 nm are observed in all three materials. Among them, Pd-GR composite exhibits the strongest absorption peak. This result suggests that the interfacial electron transfer in Pd-GR prmotes H_2O_2 activation and facilitates ROS generation.

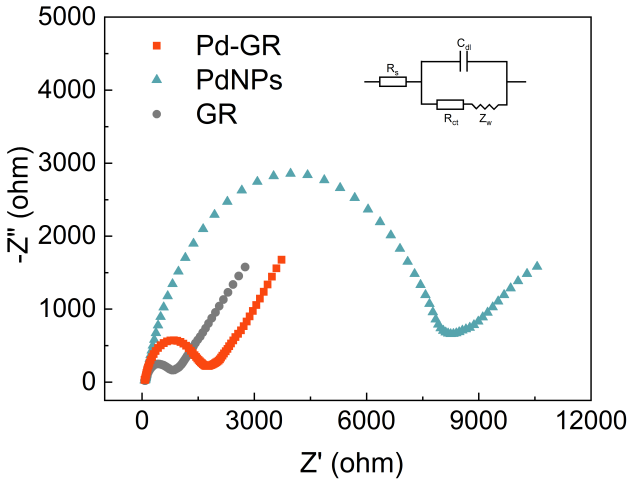

Figure S7. EIS spectra obtained at GR-, PdNPs-, and Pd-GR-modified GCE in 5.0 mM $K_3[Fe(CN)_6]/K_4[Fe(CN)_6]$ (0.1 M KCl).

We employ electrochemical impedance spectroscopy (EIS) to study the electrode reaction kinetics at the modified electrode surface. Figure S7 shows that, compared to PdNPs, Pd-GR composite exhibits a significantly smaller charge transfer resistance, indicating

faster electron transfer kinetics. The reduction in charge transfer resistance is ascribed to the two factors: 1). the increased conductivity of PdNPs due to the addition of GR; 2). the EMSI-induced redistribution of electrons at the interface between PdNPs and GR, which further accelerates charge transfer during the reaction process. This finding is consistent with the superior catalytic performance observed for Pd-GR composite in the ECL and peroxidase-like activity experiments.

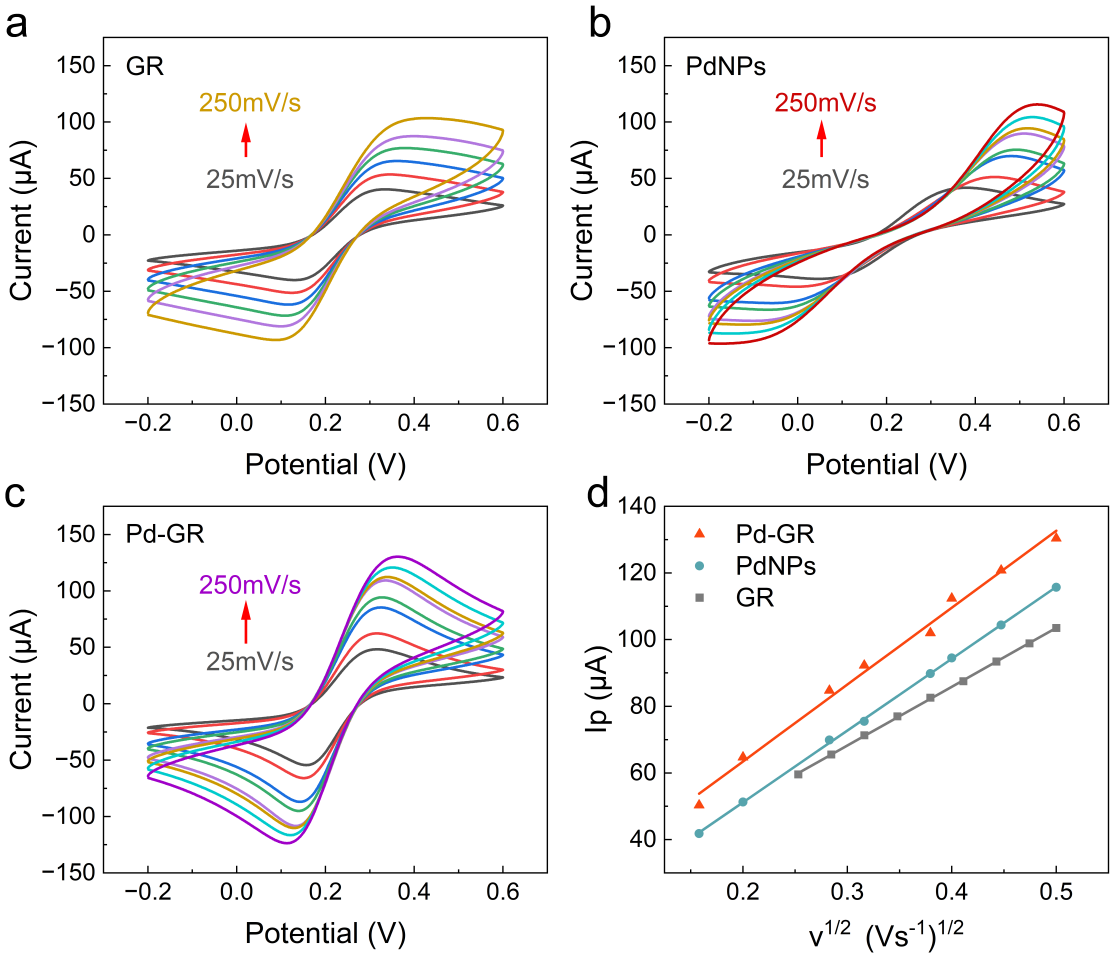

Figure S8. CV curves of (a) GR-, (b) PdNPs-, and (c) Pd-GR-modified GCE in 5.0 mM $K_3[Fe(CN)_6]/K_4[Fe(CN)_6]$ (0.1 M KCl), with a potential range from -0.2 V to 0.6 V and scanning rate from 0.025 V/s to 0.25 V/s. (d) Calibration curves of the peak current Ip against the square root of the scan rate $v^{1/2}$ for the GR-, PdNPs-, and Pd-GR-modified GCE in 5.0 mM $K_3[Fe(CN)_6]/K_4[Fe(CN)_6]$ (0.1 M KCl).

Additionally, electrochemical surface area (ECSA) analysis of GR-, PdNPs-, Pd-GR-modified GCE using the $[Fe(CN)_6]^{3-/4-}$ probe was carried out.[8] In the CV scans, the oxidation peak current of $[Fe(CN)_6]^{4-}$ increases as the increase of the scan rate from 0.025 V/s to 0.25 V/s (Figure S8 a-c). From the CV results, a linear relationship between the peak

current Ip and the square root of the scan rate $v^{1/2}$ was obtained (Figure S8d). According to the Randles-Sevcik equation:[9] $Ip = 2.69 \times 105\ n^{3/2} AD^{1/2} v^{1/2}C_0$, where n is the number of electrons for the reaction, A is the apparent electrode area [cm^2], D is the diffusion coefficient of the redox probe [$cm_2\ s^{-1}$], v is the CV scanning rate [$V\ s^{-1}$], and C_0 is the bulk concentration of $[Fe(CN)_6]^{3-/4-}$ [$mol\ cm^{-3}$]. Herein, n = 1 and D is assigned to be 1×10^{-5} $cm_2\ s^{-1}$.[10] Thus, the calculated ECSA of Pd-GR is 6.628 mm^2, which is larger than that of GR (5.066 mm^2) and PdNPs (6.190 mm^2). The increased ECSA suggests a higher density of active sites for catalytic reactions, further explaining the enhanced catalytic performance of the Pd-GR composite. Surprisingly, GR has the lowest ECSA, although GR has a large specific surface area. This result, taken together with the EIS results, suggests that the metal-support electronic interaction resulting from the combination of PdNPs and GR enhances the charge transfer rate and electrochemical active surface area of PdNPs, improves its catalytic performance for luminol oxidation and H_2O_2 activation, and consequently leads to increased ECL signal.

15. UPS spectra of GR, PdNPs, and Pd-GR

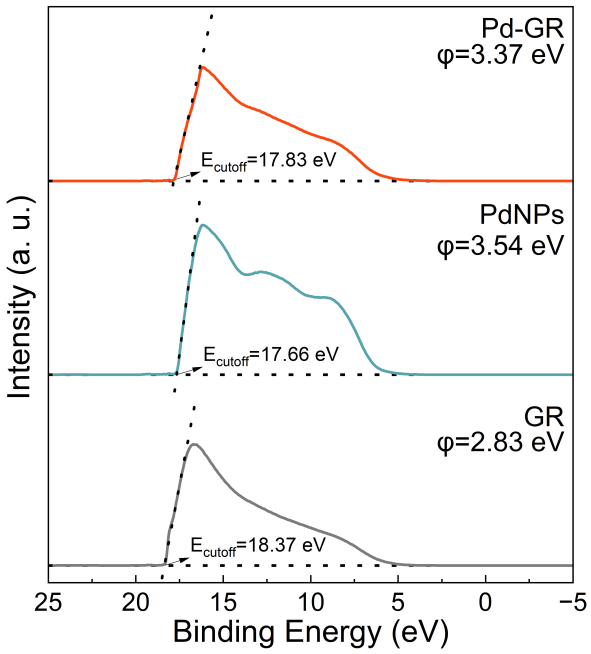

Figure S9. UPS spectra and work function of GR, PdNPs, and Pd-GR. The applied bias voltage is -5 V.

16. Structure model of Pd-GR composite for the DFT calculations

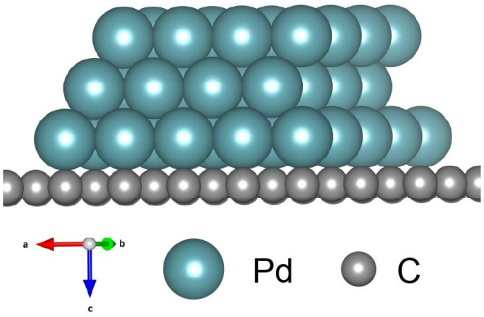

Figure S10. Schematic of the structure model of Pd-GR for the DFT calculations.

17. Detection of glucose in urine

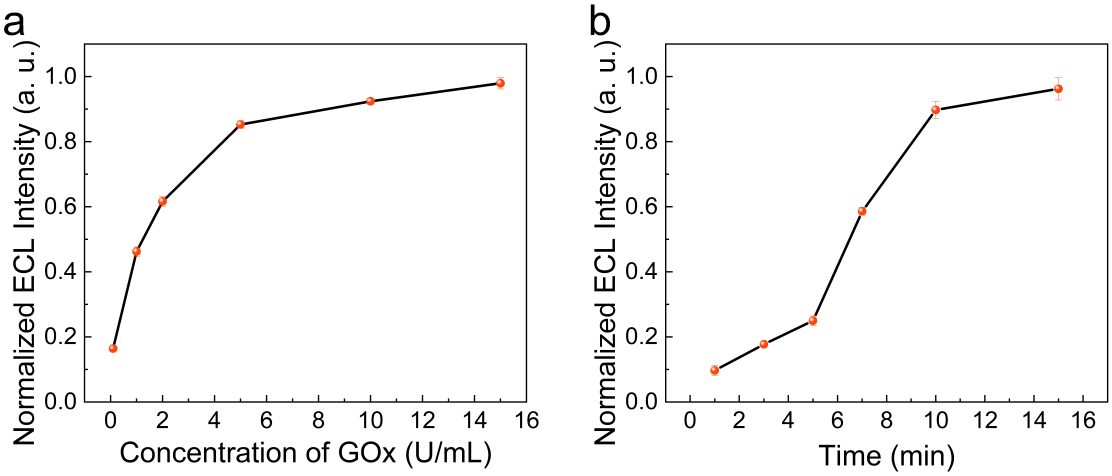

Figure S11. (a) Effect of GOx concentration on the ECL intensity of Pd-GR-modified GCE in enzymatic reaction solution of PBS buffer (pH 7.5) containing 1000 nM glucose with an incubation time of 10 min. (b) Effect of enzymatic reaction time on ECL intensity of Pd-GR-modified GCE in PBS buffer solution (pH 7.5) containing 1000 nM glucose and 5 U/mL GOx. The ECL measurements were performed in BR buffer (pH 10.0) containing 0.2 mM luminol. PMT was biased at -600 V.

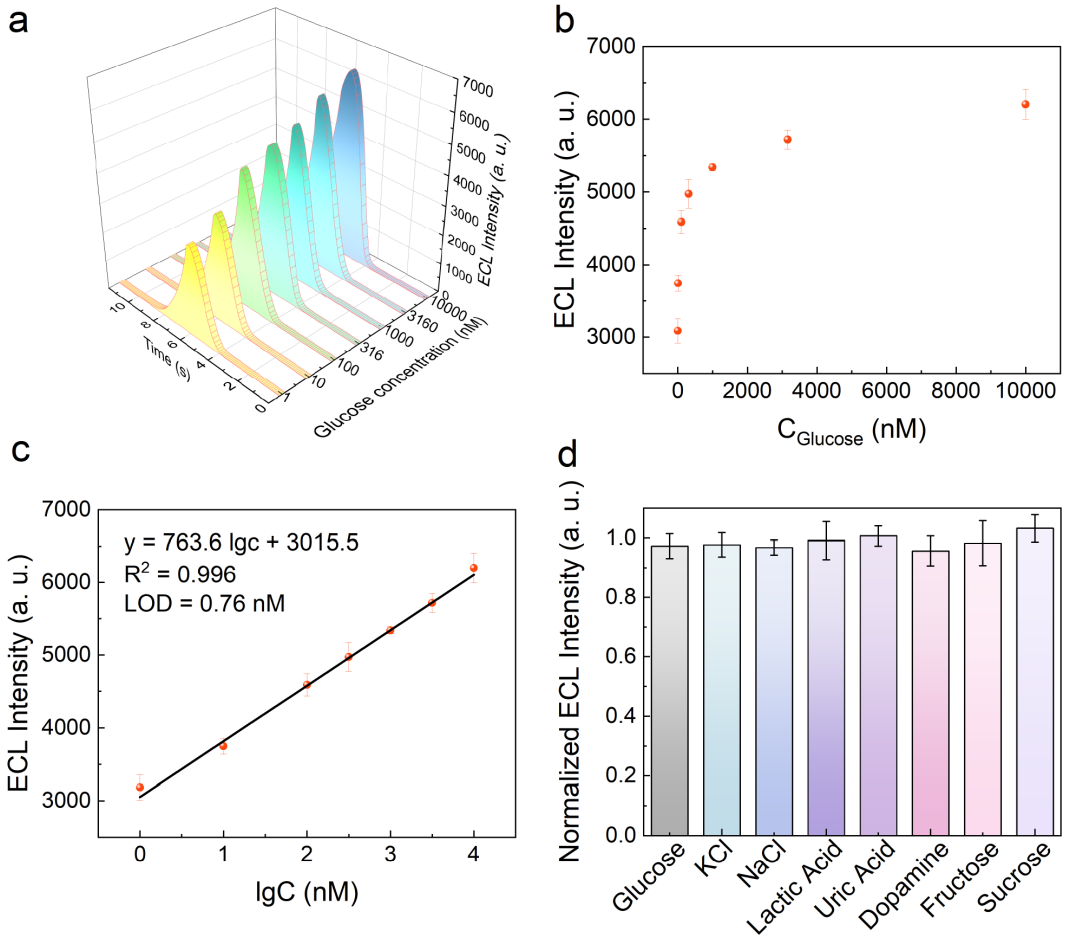

Figure S12. (a) ECL intensity-time curves obtained at Pd-GR-modified GCE in BR buffer solution (pH 10.0) containing 0.2 mM luminol and 5 U/mL of GO_x with different concentrations of glucose (from 1 nM to 10000 nM). (b) Plot of the ECL intensity shown in panel a versus glucose concentration. (c) Linear relationship between the ECL intensity and the logarithm of glucose concentrations in the Pd-GR-based ECL system. (d) Selectivity assessment of the sensor for glucose detection with various interferents. PMT was biased at -600 V.

Current diabetes diagnosis primarily relies on blood glucose concentration measurements,[11,12] a method that is invasive and can cause discomfort to patients.[13] In contrast, non-invasive detection using urine samples offers a promising alternative, as studies have demonstrated a correlation between urine glucose and blood glucose levels.[14] This non-invasive approach is particularly appealing for continuous monitoring of diabetic patients. Building on this, we developed a sensitive ECL sensor using Pd-GR composites for glucose detection. The sensor leverages the enzymatic reaction between glucose oxidase (GO_x) and glucose to generate hydrogen peroxide (H_2O_2), which in turn enhances the ECL signal.

The concentration of GO_x and the incubation time were first optimized to improve the glucose detection performance of Pd-GR composite. Figure S11a shows that the ECL intensity increased as the GO_x concentration increased, plateauing at 5

U/mL in phosphate-buffered saline (PBS) solution at pH 7.5. Therefore, 5 U/mL of GO_x was chosen for further experiments. Similarly, the incubation time of GO_x with the sample was optimized (Figure S11b). The ECL signal continued to increase with longer incubation times, but after 10 minutes, the rate of ECL increase slowed. Thus, a 10-minute incubation period was selected for its balance of efficiency and time-saving.

The performance of the sensor toward glucose detection was analyzed under optimal conditions. Glucose solutions at varying concentrations were incubated under the same conditions, and their ECL signals were measured. The results show that the ECL intensity increases with the glucose concentration (Figures S12a, b), demonstrating the sensor's sensitivity. Notably, a linear relationship between the ECL intensity and the logarithm of glucose concentration (lgc) was established in the concentration range of 1 nM to 10 μM (Figure S12c). The linear equation is I_{ECL} = 763.6 lgc + 3015.5 (where I_{ECL} is the ECL intensity and c is the glucose concentration), with a correlation coefficient (R^2) of 0.996. The limit of detection (LOD) was determined to be 0.8 nM (S/N=3), a value significantly lower than other reported glucose detection methods (Table S1). We note that the limit of detection (LOD) can be influenced by multiple factors, including electrode modification procedure, luminol/H_2O_2 concentrations, and sample matrix. Nevertheless, under the present experimental conditions, the EMSI effect in the Pd-GR composite provides an important signal-amplification mechanism that contributes to the improved sensitivity. Compared with conventional ECL catalysts, the EMSI effect in the Pd-GR composite significantly improves charge transfer efficiency and catalytic activity through interfacial electron redistribution. The electron-enriched Pd sites facilitate luminol oxidation and H_2O_2 activation. Simultaneously, graphene provides efficient electron transport pathways and promotes luminol enrichment at the interface through its large π-conjugated surface, thereby accelerating enhancing the ECL reaction efficiency. The synergistic effect between GR and PdNPs shortens the electron/mass transfer distance and thus markedly amplifies the ECL signal, which contributes to the improved analytical sensitivity and lower detection limit. The outstanding sensitivity makes it a highly promising platform for glucose detection in low-concentration environments, such as urine.

Anti-interference studies were conducted to evaluate the sensitivity of the glucose sensor. Various common interferents were tested, including inorganic salts (KCl, NaCl), small molecules (lactic acid, uric acid, and dopamine), and other sugars (fructose and sucrose). As shown in Figure S12d, the tested interferents at certain concentrations show negligible interference with glucose detection, demonstrating high selectivity toward glucose. The high selectivity is particularly valuable for real-world applications, where a range of potentially interfering substances may be present. To demonstrate the practical application of this glucose detection method, the Pd-GR sensor was used to measure the glucose concentration of urine samples of healthy individuals without any pretreatment, aside from dilution. Additionally, we conducted recovery tests in human urine samples. As summarized in Table S2, the obtained

recovery rate for the urine samples ranged from 98.2% to 102.0%, demonstrating the feasibility of using this sensor for real-time glucose analysis in urine. The low relative standard deviation (RSD) values further confirm the reliability and reproducibility of the sensor in complex biological samples.

Table S1. Summary of the test results for the detection of Glucose using different methods.

Materials	Linear range (μM)	LOD (μM)	Reference
TA-AuNPs	200-350	10.0	[15]
Pt-Pd/rGO	20-5000	8.1	[13]
MoS_2/Pd	5-2000	0.9	[16]
$ZnFe_2O_4$/GQDs	5-500	7.0	[17]
Pd-GR	0.001-10	0.00076	This work

Table S2. Glucose spiked recovery in human urine samples (diluted 100 times).

Samples	Added (nM)	Found (nM)	Recovery (%)	RSD (*n*=3, %)
1	40	40.8	102.0	5.8
2	400	392.9	98.2	2.8
3	4000	4003.9	100.1	3.3

18. References

1 S. J. Hwang, S. K. Kim, J. G. Lee, S. C. Lee, J. H. Jang, P. Kim, T. H. Lim, Y. E. Sung and S. J. Yoo, *J. Am. Chem. Soc.*, 2012, 134, 19508-19511.

2 X. Wang, S. Li, Z. Yuan, Y. Sun, Z. Tang, X. Gao, H. Zhang, J. Li, S. Wang, D. Yang, J. Xie, Z. Yang and Y. M. Yan, *Angew. Chem. Int. Ed.*, 2023, 62, e202303794.

3 A. Klinkova, E. M. Larin, E. Prince, E. H. Sargent and E Kumacheva, *Chem. Mater.*, 2016, 28, 3196-3202.

4 G. Kresse, J. Furthmüller, *Phys. Rev. B*, 1996, 54, 11169-11186.

5 J. P. Perdew, K. Burke and M. Ernzerhof, *Phys. Rev. Lett.*, 1996, 77, 3865-3868.

6 Y. Zhou, Y. Wu, Z. Luo, L. Ling, M. Xi, J. Li, L. Hu, C. Wang, W. Gu and C. Zhu, *J. Am. Chem. Soc.*, 2024, 146, 12197-12205.

7 F. Abbas, Z. Dong, A. M. A. Alboull, H. Liu, T. Eticha, W. Gao, Y. Tian and G. Xu, *Bioelectrochemistry*, 2026, 167, 109061.

8 Y. Jia, X. Fan, J. Yu, F. Lu, Z. Yuan and C. Lu, *Anal. Chem.*, 2024, 96, 5598-5607.

9 J. Lu, L. T. Drzal, R. M. Worden and I. Lee, *Chem. Mater.*, 2007, 19, 6240-6246.

10 L. L. Li, K. P. Liu, G. H. Yang, C. M. Wang, J. R. Zhang and J. J. Zhu, *Adv. Funct. Mater.*, 2011, 21, 869-878.

11 Q. Huang, J. Chen, Y. Zhao, J. Huang and H. Liu, *Talanta*, 2025, 281, 126897.

12 Y. Sun, P. Li, Y. Zhu, X. Zhu, Y. Zhang, M. Liu and Y. Liu, *Biosensors and Bioelectronics*, 2021, 194, 113600.

13 C. Chen, R. Ye, Z. Chen, J. Ye, B. Ran, B. Liu, J. Liang, J. Huang and T. Shen, *Anal. Methods*, 2025, 17, 6326-6335.

14 F. Cui, H. Sun, X. Yang, H. Zhou, Y. Wu, J. Li, H. Li, J. Liu, C. Zeng, B. Qu, J. Zhang and Q. Zhou, *Chemical Engineering Journal*, 2023, 457, 141303.

15 C. H. Peng, T. Y. Wang, C. Y. Chueh, T. Wu, J. P. Chou, M. Y. Wu and Y. W. Lin, *ACS Omega*, 2024, 9, 38217-38226.

16 Y. Liu, Z. Fu, X. Zhong, H. Song, J. Wang, G. Zhu, J. Wang and X. Ouyang, *J. Mater. Sci.*, 2025, 60, 17580-17592.

17 C. Cirillo, M. Iuliano and M. Sarno, *Micromachines*, 2025, 16, 520-541.